Computer Methods in Biomechanics and Biomedical Engineering

Effect of spatial inlet velocity profiles on the vortex formation pattern in a dilated left ventricle

Bee Ting Chan [a] , Einly Lim [a] , Chi Wei Ong [a] & Noor Azuan Abu Osman [a]

[a] Department of Biomedical Engineering , Faculty of Engineering, University of Malaya , 50603 , Kuala Lumpur , Malaysia
Published online: 22 Mar 2013.

PLEASE SCROLL DOWN FOR ARTICLE

Taylor & Francis
Taylor & Francis Group

Effect of spatial inlet velocity profiles on the vortex formation pattern in a dilated left ventricle

Bee Ting Chan*, Einly Lim[1], Chi Wei Ong[2] and Noor Azuan Abu Osman[3]

Department of Biomedical Engineering, Faculty of Engineering, University of Malaya, 50603 Kuala Lumpur, Malaysia

Despite the advancement of cardiac imaging technologies, these have traditionally been limited to global geometrical measurements. Computational fluid dynamics (CFD) has emerged as a reliable tool that provides flow field information and other variables essential for the assessment of the cardiac function. Extensive studies have shown that vortex formation and propagation during the filling phase acts as a promising indicator for the diagnosis of the cardiac health condition. Proper setting of the boundary conditions is crucial in a CFD study as they are important determinants, that affect the simulation results. In this article, the effect of different transmitral velocity profiles (parabolic and uniform profile) on the vortex formation patterns during diastole was studied in a ventricle with dilated cardiomyopathy (DCM). The resulting vortex evolution pattern using the uniform inlet velocity profile agreed with that reported in the literature, which revealed an increase in thrombus risk in a ventricle with DCM. However the application of a parabolic velocity profile at the inlet yields a deviated vortical flow pattern and overestimates the propagation velocity of the vortex ring towards the apex of the ventricle. This study highlighted that uniform inlet velocity profile should be applied in the study of the filling dynamics in a left ventricle because it produces results closer to that observed experimentally.

Keywords: computational fluid dynamics; velocity profile; vortex; dilated cardiomyopathy

Introduction

Dilated cardiomyopathy (DCM) is the most common cardiomyopathy disease, which leads to heart failure and mortality. The hallmark of DCM is ventricular chamber enlargement and myocardial contractile dysfunction (Jefferies and Towbin 2010). DCM can be caused by many factors, such as genetic, infection, alcohol abuse and other cardiac diseases. Generally, the aetiology of DCM is classified into ischaemic and non-ischaemic. Ischaemic DCM occurs with poor perfusion of the myocardial wall due to coronary disease. Among the non-ischaemic group, idiopathic DCM is the most common. It arises spontaneously and has unknown causes. Irrespective of the disease aetiology, all DCM patients experience similar mechanical compensation. This study focuses on the intracardiac flow variables in the left ventricle (LV) with idiopathic DCM.

Intraventricular flow distribution in the heart chamber infers important information, which is particularly useful in the assessment of cardiac health. Cardiac magnetic resonance imaging (MRI) and echocardiography have been extensively used to evaluate cardiac flow field due to their non-invasive nature. For instance, redirection of flow and vortex structure has been observed in the human heart during the filling phase through echocardiography (Garcia et al. 1998; Hong et al. 2008) and magnetic resonance velocity mapping (Kilner et al. 2000).

Vortex formation in the LV has been widely investigated through various experiments and was found to be closely related to the mechanism of atrial systole and the movement of the valves (Bellhouse 1972; Dahl et al. 2012). On the other hand, extensive computational fluid dynamics (CFD) studies using patient-specific models (Saber et al. 2001; Schenkel, Krittian et al. 2009) and more advanced fluid structure interaction models (Watanabe et al. 2002; Cheng et al. 2005; Krittian et al. 2010) have been performed to investigate the correlation between vortex patterns and cardiac performance. Besides showing vortex ring formation in the ventricle, a few parameters related to the vortex ring including propulsion velocity, vorticity strength and energy dissipation have been found to be closely related to the ventricular function. Consequently, it was suggested that vortex patterns in the ventricle serves as a useful indicator of cardiac health (Gharib et al. 2006).

Further investigations revealed that geometrical alteration of the LV induces changes in the blood flow pattern (Ge and Ratcliffe 2009). Blood flow patterns were inspected in DCM patients using both colour Doppler echocardiography (D'cruz and Sharaf 1991; Thomas et al. 2009) and CFD models (Baccani et al. 2002b; Doenst et al. 2009). The distortion of the geometrical heart shape in these patients produced abnormal vortical flow patterns, where vortex formation and propagation speed are reduced significantly, leading to a stagnant flow area in the apical region, which potentially induces thrombus formation. However, most CFD studies on LV with DCM did not mention the

---

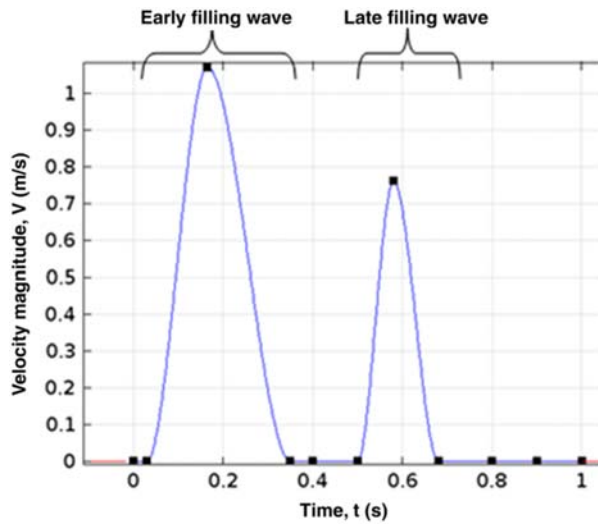*Corresponding author. Email: beetn_chan@yahoo.com

Figure 1. Temporal profile of inlet velocity in a cardiac cycle.

velocity profile of the transmitral blood flow used in their studies.

In any CFD study, proper settings of geometry, fluid properties, boundary conditions and mesh are of utmost importance (Lee 2011). Improper boundary condition contributes to inaccuracy in the results, leading to wrong diagnosis of cardiac health. Therefore, the aim of this article is to examine the effect of inlet velocity profile, i.e. the transmitral velocity profile (parabolic and uniform velocity profile) on the vortex formation patterns in an LV with DCM.

Method

The LV is modelled using an axisymmetrical truncated prolate spheroid with a diameter D of 6 cm and a height H of 9.5 cm to represent an idiopathic DCM condition with

an end diastolic volume of 180 ml. The mitral valve is located at the base of the LV characterised by an opening orifice with a diameter of 2.5 cm. Since the focus of this study is on the diastolic phase, the aortic valve is closed throughout the simulation. The blood is assumed to be incompressible and Newtonian with a viscosity of 0.0035 Pa s and a density of 1050 kg/m³. The blood flows into the LV through the mitral orifice. The temporal profile of the inlet velocity in one cardiac cycle, obtained through University Malaya Medical Centre (UMMC) from a DCM patient, as shown in Figure 1 is applied at the mitral orifice as the inlet boundary condition. Physiologically, the *E* wave (first wave) is induced by a pressure gradient between the left atrium and the LV, while the *A* wave (second wave) is due to atrial contraction.

Two different laminar velocity profiles are imposed across the mitral orifice: uniform velocity profile and parabolic velocity profile. Figure 2 shows the spatial profile of the inlet velocity at the mitral valve at $t = 0.17$ s (when peak velocity occurs). The velocity is constant at 1.07 m/s throughout the mitral valve using the uniform velocity profile setting. Using the parabolic velocity profile setting, the highest velocity occurs at the middle of the valve where the peak velocity magnitude is 2.063 m/s.

The LV wall is modelled as impermeable. No slip boundary condition is imposed, where the blood flow velocity along the wall is zero relative to the wall movement, as described in Equation (1):

$$\mathbf{v}_{\text{fluid}} = \mathbf{v}_{\text{wall}}, \tag{1}$$

where $\mathbf{v}_{\text{fluid}}$ (m/s) is the fluid velocity vector, and $\mathbf{v}_{\text{wall}}$ (m/s) is the wall velocity vector.

The quantitative blood flow dynamics is solved using the continuity (2) and incompressible Navier–Stokes
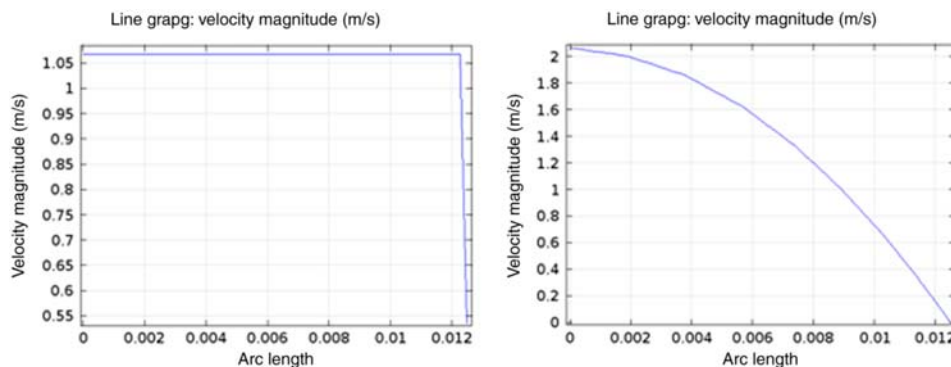

Figure 2. Spatial profile of inlet velocity at the mitral valve at $t = 0.17$ s, using different settings: uniform flow (left) and parabolic flow (right). Figure shows only half of the valve diameter due to the axisymmetric representation, where arc length = 0 represents middle of the valve, while arc length = 0.0125 represents edge of the valve.

Equations (3),

$$\nabla \cdot \mathbf{v} = 0, \qquad (2)$$

$$\rho\left(\frac{\delta \mathbf{v}}{\delta t} + \mathbf{v} \cdot \nabla \mathbf{v}\right) = -\nabla p + \mathbf{F} + \mu \nabla^2 \mathbf{v}, \qquad (3)$$

where $\mathbf{v}$ (m/s) is the fluid velocity vector, ρ (kg/m³) the fluid density, p (Pa) the pressure and μ (Pa s) is the fluid viscosity. The numerical calculation is solved using the Newton–Raphson method in the COMSOL software (COMSOL, Inc, Burlington, MA, US).

During the filling phase, the volume of the enclosed LV is increased. Thus, a prescribed ventricular wall motion is required in order to obey the mass conservation principle. We adapt the method proposed by Baccani et al. (2002b), where the wall motion is derived from the instantaneous blood flow rate $Q(t)$ (m³/s) through the mitral valve on the basis of a simple elastic membrane model. The rate of change of the radius, R (m), and the height, H (m), are

$$\frac{dR}{dt} = \frac{3Q(t)}{\pi} \frac{2H^2 - R^2}{10H^3R - 4HR^3} \qquad (4)$$

$$\frac{dH}{dt} = \frac{3Q(t)}{\pi} \frac{H^3}{2H^2R - R^3} \frac{2H^2 - R^2}{10H^3R - 4HR^3}. \qquad (5)$$

Results

Two types of laminar inlet velocity profiles are simulated during the filling phase: uniform and parabolic profiles. The results were analysed based on the vorex evolution pattern and vortex strength.

Vortex evolution pattern

Although blood flows across the narrow mitral orifice to the broader ventricular chamber, blood decelerates and pressure increases simultaneously in the direction of flow according to the conservation of mass and Bernoulli's principle. The higher pressure at the downstream opposes the incoming flow stream, leading to a fan-like flow towards the ventricular wall. As a result, the flow stream tends to roll up and redirect towards the mitral valve (Pasipoularides et al. 2003).

Distinct vortex evolution patterns are observed between the two cases: transmitral flow velocity with uniform (Figure 3) and parabolic inlet velocity profiles (Figure 4). In the ventricle with a uniform inlet velocity profile, the incoming flow stream is rolled up immediately after travelling through a short distance away from the mitral valve ($t = 0.15$ s). The redirected blood stream

Figure 3. Vortex formation patterns obtained using uniform velocity profile as inlet boundary condition at $t = 0.15$ s (left), 0.25 s (middle) and 0.35 s (right).

forms a vortex ring, preserving the kinetic energy of the incoming flow through the fast spinning velocity. The attachment of the vortex ring attached at the mitral edge restricts its propagation. Although the attached vortex ring is still able to move closer to the lateral wall in the meantime towards the apex, its low vortex strength does not help to break the wake attachment at the mitral edge. The uniform flow stream hanging at the basal region experiences a small convective acceleration that is unable to overcome the local deceleration effect.
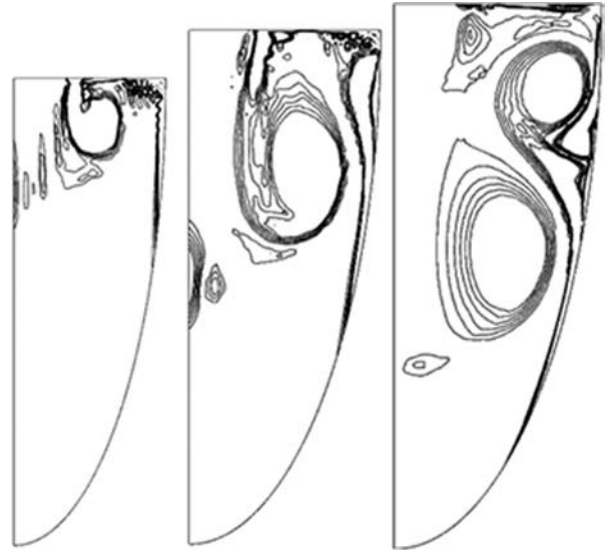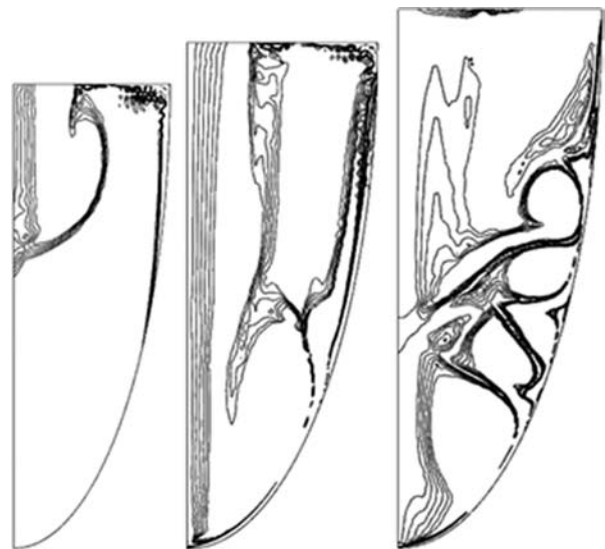

Figure 4. Vortex formation patterns obtained using parabolic velocity profile as inlet boundary condition at $t = 0.15$ s (left), 0.25 s (middle) and 0.35 s (right).

During deceleration of the transmitral velocity ($t = 0.25$ s), kinetic energy decreases at the basal region, while pressure decreases at the apical region. The change in the pressure and the velocity encourages the growth of the vortex ring and facilitates its detachment from the attached wake at a later time. The free vortex ring starts to propagate at self-induced convection against the higher pressure at the apical region. Meanwhile, it interacts with the ventricular wall and induces the formation of another small vortex ring that developed from a boundary layer. The high-pressure energy at the apical region and low vortex strength or kinetic energy of the propagating flow stream restrict the penetration of the vortex ring to the end of the apex in the enlarged chamber. As a result, the vortex ring halts at the mid-ventricular region ($t = 0.35$ s). The region beneath the vortex ring remains in a low-velocity condition. The same vortex evolution process reprises during late filling. The secondary vortex ring was produced in smaller size due to the low inflow volume.

Conversely, the parabolic flow stream containing high kinetic energy propels the flow stream towards the apex. The parabolic flow stream travels under great inertial influence and is therefore able to approach the middle region of the LV during the acceleration phase ($t = 0.15$ s). No vortex ring is developed in the early filling phase because the flow stream is able to overcome the high pressure at the apical region without being redirected towards the base. The incoming fluid propagates against the resistance of the resting fluid and develops a shear layer. During deceleration of the transmitral velocity ($t = 0.25$ s), the parabolic flow stream is decelerated progressively by the accumulated pressure energy deposited in the resting fluid and local deceleration at the down-stroke of the E wave. However, at this moment, the parabolic flow stream, which has already reached the lower part of the ventricle, experiences a convective acceleration at the same time due to the decreasing diameter of the ventricle at the apex ($t = 0.25$ s). Once the energetic parabolic flow comes in contact with the myocardial wall at the end of the apex, the flow stream is reflected and redirected towards the basal region. As a consequence of the interaction between the flow stream and the myocardial wall, a boundary layer is formed near the wall, which contains vorticity rotating in opposite direction with that of the parabolic flow. This boundary layer develops into small vortices that interact among each other and with the ventricular wall to produce strong vorticity as observed during diastasis ($t = 0.35$ s). The same process is repeated during the late filling phase.

Vortex strength

The instantaneous vortex strength in both the uniform and parabolic flow studies is shown in Figure 5, where the maximum vortex strength in the LV with a parabolic inlet
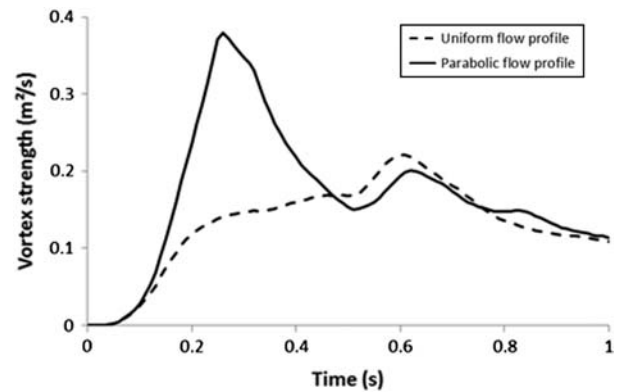

Figure 5.   Vortex strength in a DCM ventricle with different spatial velocity profile.

velocity profile (0.38 m^2/s) is almost two times greater than that using a uniform inlet velocity profile (0.22 m^2/s). The maximum vortex strength occurs during early filling in the first scenario (using a parabolic inlet velocity profile) but during late filling in the second scenario (using a uniform inlet velocity profile).

Discussion

The vortex evolution pattern acts as an important cardiac health assessment because it reveals the risk of apical thrombosis in the dilated ventricle (Maze et al. 1989). Several studies have been carried out to investigate the effect of the intraventricular vortex flow pattern on the normal (Vierendeels et al. 2000; Baccani et al. 2002a) and the diseased ventricles (Baccani et al. 2002b; Pasipoular-ides et al. 2003; Domenichini and Pedrizzetti 2011), using echocardiography (D'cruz and Sharaf 1991) and MRI (Schenkel, Malve et al. 2009) as validation tools. In a normal ventricle, the incoming flow is redirected towards the base by the higher pressure at the downstream, thus forming a vortex ring attaching to the mitral edge. During deceleration of the E wave, this vortex ring is detached from the mitral edge and moves freely towards the apex region with a high vortex strength. As a result, the vortex ring is able to reach the end of the LV apex during the filling phase (Vierendeels et al. 2000; Baccani et al. 2002b). On the contrary, the vortex movement is restricted in a DCM ventricle due to a longer period of vortex attachment at the mitral edge. The DCM ventricle produces a lower vortex strength, which is insufficient to propagate the vortical flow towards the bottom of the LV (Chan et al. 2012).

In this study, vortex formation pattern in the LV with a uniform inlet velocity profile agrees with that reported in the literature, where the vortex ring is attached to the mitral edge until the diastasis phase. In addition, instead of moving vertically downwards, towards the apex as observed in the LV with a parabolic inlet velocity profile,

the vortex ring is enlarged in the dilated LV and extended axially towards the side wall of the ventricle (Garcia et al. 1998; Baccani et al. 2002b). As a result, the vortex ring is not able to reach the end of the apex to wash out the apical stagnant flow, leading to an increase in the risk of thrombus formation at the apex. Conversely, simulation study using a parabolic inlet velocity profile yields a deviated vortex pattern compared with that observed clinically, where the incoming flow travels straight down to the end of the apex with a higher vortex strength.

The difference in the vortex formation pattern and vortex strength using the two different spatial inlet velocity profiles can be explained through the use of the kinetic energy factor, α (Cengel and Cimbala 2006), i.e. the ratio of the actual kinetic energy. With an identical average inflow rate, parabolic flow stream travels with a maximum velocity (2.06 m/s, at the middle of the LV) of about twice that of the uniform flow stream (1.07 m/s), as seen in Figure 2, although both velocity profiles have comparable average velocity. In a laminar flow condition, the kinetic energy factor, which is associated with the spatial velocity profile, is extremely important because it affects the kinetic energy and the velocity of the flow stream. Detailed derivations of the kinetic energy factor, α, for both the uniform and parabolic inlet velocity profiles, are given in Appendix. It is shown that the parabolic inlet velocity profile produces a kinetic energy factor, which is two-fold higher compared with that using the uniform inlet velocity profile.

Although maximum vortex strength occurs during early filling (0.26 s) in LV with parabolic inlet velocity profile, it happens during late filling (0.6 s) in LV with flat inlet velocity profile. During early filling, the energetic parabolic inlet flow penetrates rapidly through the ventricular chamber and knocks on the apical wall. The interaction between the reflected flow stream and the myocardial wall produces intense vortices, therefore high vortex strength. On the contrary, the lower energetic flat inlet flow propagates slower and remains at the basal region during early filling, resulting in less interaction between the vortex ring and the wall. However, as vortex propagates towards the apical region, vortex strength increases and exceeds that in LV with parabolic inlet velocity profile during late filling. During this period, vortex strength has reduced in LV with parabolic inflow due to the heat and viscous dissipation losses.

Model limitation

In this preliminary study, the LV is modelled with a simplified geometry with the absence of the left atrium, mitral leaflets and the papillary muscle. The intracardiac flow disturbance potentially created by the existence of the papillary muscles is not evaluated. In addition, the LV is modelled using the axisymmetrical approach. Therefore, we are not able to

simulate the asymmetric vortex profile occurring in the LV, which may help to avoid the stagnant area in the ventricular apex [Schenkel, Krittian et al. 2009]. The ventricular movement in this model is prescribed as a simple expansion without including the twisting motion of the LV and the wall compliance. A normal filling pattern is used in this study rather than the impaired and restrictive filling pattern observed in DCM patients in severe stage (Nishimura and Tajik 1997). However, since the main objective of this study is to compare the influence of the spatial profile of the transmitral velocity on the vortex formation patterns, these limitations do not affect the outcome of the comparison analysis.

Conclusion

When blood enters the LV from the mitral valve, the change of the geometrical dimensions and the short mitral valve length disables the laminar blood flow to be fully developed into a parabolic profile. As a result, incoming blood enters the LV with a uniform velocity profile during the filling phase. It is shown from this study that the transmitral velocity profile significantly affects the intraventricular vortex flow pattern. The resulting vortex evolution pattern using the uniform inlet velocity profile agreed with that reported in the literature, which revealed an increase in thrombus risk in a ventricle with DCM. On the contrary, the application of a parabolic velocity profile at the inlet yields a deviated vortical flow pattern and overestimates the propagation velocity of the vortex ring towards the apex of the ventricle.

Notes

1. Email: einly_lim@um.edu.my
2. Email: chiweiong@gmail.com
3. Email: azuan@um.edu.my

References

Baccani B, Domenichini F, Pedrizzetti G, Dirk LB. 2002a. Vortex dynamics in a model left ventricle during filling. Eur J Mech B Fluids. 21:527–543.

Baccani B, Domenichini F, Pedrizzetti G, Tonti G. 2002b. Fluid dynamics of the left ventricular filling in dilated cardiomyopathy. J Biomech. 35:665–671.

Bellhouse BJ. 1972. Fluid mechanics of a model mitral valve and left ventricle. Cardiovasc Res. 6:199–210.

Cengel YA, Cimbala JM. 2006. Fluid mechanics: fundamentals and applications. New York: McGraw-Hill Education.

Chan B, Ong C, Lim E, Abu Osman N, Al Abed A, Lovell N, Dokos S. 2012. Simulation of left ventricle flow dynamics

with dilated cardiomyopathy during the filling phase. Paper presented at: the Engineering in Medicine and Biology Society (EMBC), 2012 Annual International Conference of the IEEE; San Diego, CA, USA.

Cheng YG, Oertel H, Schenkel T. 2005. Fluid-structure coupled CFD simulation of the left ventrivular flow during filling phase. Ann Biomed Eng. 33(5):567–576.

D'cruz I, Sharaf IS. 1991. Patterns of flow within the dilated cardiomyopathic left ventricle: color flow Doppler observations. Echocardiography. 8(2):227–231.

Dahl SK, Vierendeels J, Degroote J, Annerel S, Hellevik LR, Skallerud B. 2012. FSI simulation of asymmetric mitral valve dynamics during diastolic filling. Comput Met Biomech Biomed Eng. 15(2):121–130.

Doenst T, Spiegel K, Reik M, Markl M, Hennig J, Nitzsche S, Beyersdorf F, Oertel H. 2009. Fluid-dynamic modeling of the human left ventricle: methodology and application to surgical ventricular reconstruction. Ann Thorac Surg. 87(4):1187–1195.

Domenichini F, Pedrizzetti G. 2011. Intraventricular vortex flow changes in the infarcted left ventricle: numerical results in an idealised 3D shape. Comput Methods Biomech Biomed Eng. 14(1):95–101.

Garcia MJ, Thomas JD, Klein AL. 1998. New Doppler echocardiograhpy applications for the study of diastolic function. J Am Coll Cardiol. 32:865–875.

Ge L, Ratcliffe M. 2009. The use of computational flow modeling (CFD) to determine the effect of left ventricular shape on blood flow in the left ventricle. Ann Thorac Surg. 87:993–994.

Gharib M, Rambod E, Kheradvar A, Sahn DJ, Dabiri JO. 2006. Optimal vortex formation as an index of cardiac health. Proc Natl Acad Sci USA. 103(16):6305–6308.

Hong GR, Pedrizzetti G, Tonti G, Li P, Wei Z, Kim JK, Baweja A, Liu S, Chung N, Houle H, et al., 2008. Characterization and quantification of vortex flow in the human left ventricle by contrast echocardiography using vector particle image velocimetry. J Am Coll Cardiol. 1(6):705–717.

Jefferies JL, Towbin JA. 2010. Dilated cardiomyopathy. Lancet. 375(9716):752–762.

Kilner PJ, Yang GZ, Wilkes AJ, Mohiaddin RH, Firmin DN, Yacoub MH. 2000. Asymmetric redirection of flow through the heart. Nature. 404:759–761.

Krittian S, Janoske U, Oertel H, Bohlke T. 2010. Partitioned fluid-solid coupling for cardiovascular blood flow. Ann Biomed Eng. 38(4):1426–1441.

Lee BK. 2011. Computational fluid dynamics in cardiovascualr disease. Kor Soc Cardiol. 41(8):423–430.

Maze S, Kotler M, Parry W. 1989. Flow characteristics in the dilated left ventricle with thrombus: qualitative and quantitative Doppler analysis. J Am Coll Cardiol. 13(4):873–881.

Nishimura RA, Tajik AJ. 1997. Evaluation of diastolic filling of left ventricle in health and disease: Doppler echocardiography is the clinician's rosetta stone. J Am Coll Cardiol. 30(1):8–18.

Pasipoularides A, Shu M, Shah A, Womack MS, Glower DD. 2003. Diastolic right ventricular filling vortex in normal and volume overload states. Am J Physiol Heart Circ Physiol. 284:H1064–H1072.

Saber NR, Gosman AD, Wood NB, Kilner PJ, Charrier CL, Firmin DN. 2001. Computational flow modeling of the left ventricle based on in vivo MRI data: initial experience. Ann Biomed Eng. 29:275–283.

Schenkel T, Krittian S, Spiegel K, Höttges S, Perschall M, Oertel H. 2009. The Karlsruhe Heart Model KaHMo: a modular framework for numerical simulation of cardiac hemodynamics. Paper presented at: the IFMBE Proceedings; Munich.

Schenkel T, Malve M, Reik M, Markl M, Jung B, Oertel H. 2009. MRI-based CFD analysis of flow in a human left ventricle methodology and application to a healthy heart. Ann Biomed Eng. 37(3):503–515.

Thomas DE, Wheeler R, Yousef ZR, Masani ND. 2009. The role of echocardiography in guiding management in dilated cardiomyopathy. Eur Heart J. 10(8):iii15–iii21.

Vierendeels J, Riemslagh K, Dick E, Verdonck P. 2000. Computer simulation of intraventricular flow and pressure gradients during diastole. J Biomech Eng. 122:667–674.

Watanabe H, Hisada T, Sugiura S, Okada J, Fukunari H. 2002. Computer simulation of blood flow, left ventricular wall motion and their interrelationship by fluid-structure interaction finite element method. JSME Int J. 45(4):1003–1011.
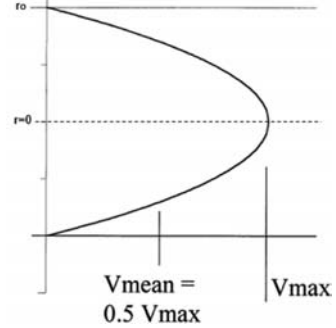
Appendix

	Uniform	Parabolic
Velocity profile	Vmax = Vmean	Vmean = 0.5 Vmax Vmax
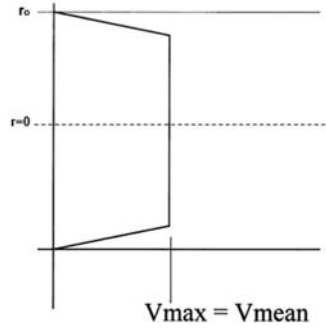
Kinetic energy correction factor, α

$$KE_{actual} = \frac{1}{2}\dot{m}_{actual}V_r^2 = \frac{1}{2}\rho\int_A V_r^3 dA$$

$$KE_{average} = \frac{1}{2}\dot{m}_{ave}V_{ave}^2 = \frac{1}{2}\rho A V_{ave}^3$$

$$\alpha = \frac{KE_{actual}}{KE_{average}} = \frac{1}{A}\int_A\left(\frac{V_r}{V_{ave}}\right)^3 dA$$

KE_{actual}: actual kinetic energy

$KE_{average}$: average kinetic energy

$\dot{m}_{actual}$: actual mass flow rate

$\dot{m}_{ave}$: average mass flow rate
A: mass flow area
V_r: spatial velocity profile
V_{ave}: average velocity
V_{max}: maximum velocity
r_o: radius of flow profile

Uniform column:

$$\alpha = \frac{KE_{actual}}{KE_{average}}$$

$$= \frac{1}{A}\int_A\left(\frac{V_r}{V_{ave}}\right)^3 dA$$

$$= \frac{1}{\pi r_o^2(V_{ave})^3}\int_0^{r_o} 2\pi r(V_r)^3 dr$$

$$= \frac{1}{\pi r_o^2(V_{max})^3}\int_0^{r_o} 2\pi r[(V_{max})]^3 dr$$

$$= \frac{2}{r_o^2}\int_0^{r_o} r dr$$

$$= \frac{2}{r_o^2}\left[\frac{r^2}{2}\right]_0^{r_o}$$

$$= \frac{2}{r_o^2}\left(\frac{r_o^2}{2}\right)$$

$$= 1$$

Parabolic column:

$$\alpha = \frac{KE_{actual}}{KE_{average}}$$

$$= \frac{1}{A}\int_A\left(\frac{V_r}{V_{ave}}\right)^3 dA$$

$$= \frac{1}{\pi r_o^2(V_{ave})^3}\int_0^{r_o} 2\pi r(V_r)^3 dr$$

$$= \frac{1}{\pi r_o^2(V_{max}/2)^3}\int_0^{r_o} 2\pi r[(V_{max})(1-(r^2/r_o^2))]^3 dr$$

$$= \frac{16}{r_o^2}\int_0^{r_o} r\left(1-\frac{r^2}{r_o^2}\right)^3 dr$$

$$= -\frac{8}{4}\left[\left(1-\frac{r^2}{r_o^2}\right)^4\right]_0^{r_o}$$

$$= -\frac{8}{4}(-1)$$

$$= 2$$